ARTICLE

Using Spectroscopic Ellipsometry to Characterize and Apply the Optical Constants of Hollow Gold Nanoparticles

Dehui Wan, Hsuen-Li Chen,* Yu-Syuan Lin, Shang-Yu Chuang, Jiann Shieh,† and Szu-Hung Chen†

Department of Materials Science and Engineering, National Taiwan University, Taipei, Taiwan. †National Nano Device Laboratory, Hsinchu, Taiwan.

ABSTRACT In this paper, we report the optical constants (refractive index, extinction coefficient) of self-assembled hollow gold nanoparticle (HGN) monolayers determined through spectroscopic ellipsometry (SE). We prepared a series of HGNs exhibiting various morphologies and surface plasmon resonance (SPR) properties. The extinction coefficient (k) curves of the HGN monolayers exhibited strong SPR peaks located at wavelengths that followed similar trends to those of the SPR positions of the HGNs in solution. The refractive index (n) curves exhibited an abnormal dispersion that was due to the strong SPR extinction. The values of Δn and k_{max} both correlated linearly with the particle number densities. From a comparison of the optical constant values of HGNs with those of solid Au nanoparticles (NPs), we used SE measurements to demonstrate a highly sensitive Si-based chemical sensor. HGNs display a slightly lower value of k at the SPR peak but a much higher sensitivity to changes in the surrounding medium than do solid Au NPs.

KEYWORDS: hollow gold nanoparticles · refractive index · extinction coefficient · spectroscopic ellipsometry · Si-based SPR sensor

In recent years, there has been increasing interest in determining the physical properties of metal nanostructures because of their fundamental and technological applications. In particular, metal nanoparticles (NPs) are known for their ability to support resonant plasma oscillations. For example, Au NPs are attractive for their surface plasmon resonance (SPR) properties. The strong interactions of metallic NPs with incident light, that is, with the oscillating electric field, originate from the excitation of collective oscillations of conduction electrons within these particles. The collective oscillation of the electrons is called the dipole plasmon resonance of the particle.[1] The SPR frequency of a metal NP can be tuned through controlling its size,[2] shape,[3] structure,[4,5] aggregate morphology,[6] surface modification,[7] and the refractive index of surrounding medium.[8]

Moreover, hollow gold NPs (HGNs) have attracted a great deal of attention because of their unique structural and optical properties, including high surface areas, low densities, and tunable SPR features. In particular, HGNs exhibit an apparent red shift of their SPR signal relative to that of solid Au colloids. The SPR wavelength depends on the ratio of the shell thickness to its diameter.[9] In addition, the SPR wavelengths of HGNs are much more sensitive toward variations in the surrounding medium than are those of solid Au or Ag NPs.[10] This new class of metal nanostructures has a number of uses, including applications in surface-enhanced Raman scattering (SERS),[11] optical imaging,[12] and photothermal therapy.[13]

SPR techniques are now used routinely in a wide variety of chemical and biological sensors.[14−19] Of particular note, solid Au NP monolayers have been used as SPR sensors[17,18] and incorporated into an SPR chip to enhance the signal amplitude.[19] An SPR chip generally features a layer-by-layer structure; its optical performance can be simulated by determining the refractive index (n) and extinction coefficient (k) of the Au NPs. In contrast, the optical characterization of monolayer Au NPs is ambiguous and not straightforward. To determine more of the optical properties of metal NP films, spectroscopic ellipsometry (SE) has been applied to characterize assemblies of Au NPs deposited on solid substrates. Kooij *et al.* reported the optical constants of monolayer Au NPs adsorbed on Si substrates: they determined extremely small optical constants in the visible wavelength region ($n < 1.2$; $k < 0.15$).[20] Evans *et al.* also characterized the values of n and k of layer-by-layer self-assembled Au NPs; they varied from 1.46 and 0.97, respectively, at 500 nm to 2.60 and 0.98, respectively, at 650 nm.[21] These large discrepancies in the values of n resulted from the nature of the NP structures. Several other groups have also studied the relationship between the

*Address correspondence to hsuenlichen@ntu.edu.tw.

Received for review December 26, 2008 and accepted March 03, 2009.

Published online March 16, 2009.
10.1021/nn8009008 CCC: $40.75

© 2009 American Chemical Society

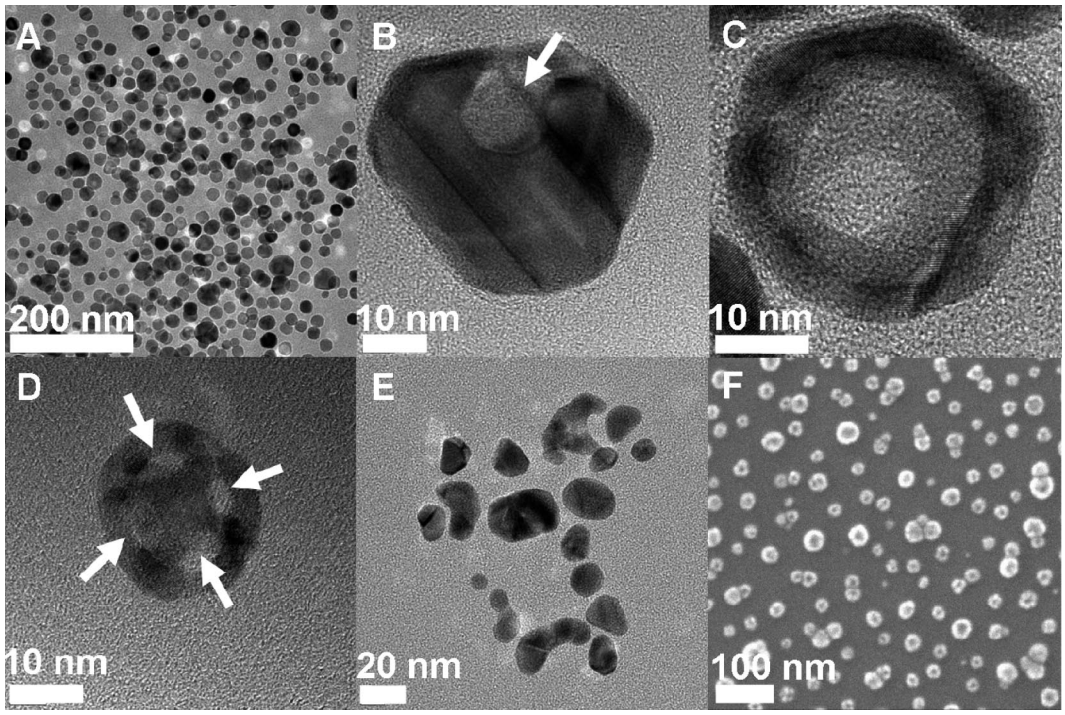

Figure 1. TEM images of (A) Ag NPs, (B−D) HGNs synthesized after reacting the Ag NPs with (B) 0.75, (C) 1.3, and (D) 1.45 mL of an aqueous $HAuCl_4$ solution, and (E) the solid Au NPs (collapsed HGNs) obtained after adding 2 mL of the $HAuCl_4$ solution to the Ag NPs. (F) Typical SEM image of an HGN monolayer on a Si substrate. The arrow in B indicates the formation of holes on the surface and the hollow nanostructure in the interior. The arrows in D indicate the pinholes and the porous surface.

optical constants and the particle density of Au NP films.[22−25] Besides, SE has also been applied to investigate the optical constants of different metals.[35,36] To date, however, no studies of the optical constant of self-assembled HGNs have been reported, especially for sensing applications.

In this paper, we report the optical constants *n* and *k* of self-assembled monolayer HGNs immobilized on substrates. We prepared various solid and hollow metal NPs through the galvanic replacement reaction between Ag NPs and $HAuCl_4$. Changing the Ag NPs-to-$HAuCl_4$ ratio allowed us to modify the SPR wavelength. To obtain the values of *n* and *k* of the monolayer HGNs, we used ellipsometry to measure the change in the polarization state of light reflected from the surface of a sample in terms of the values of Ψ and Δ. We then used the simplest three-layer model, consisting of the ambient, NP layer, and substrate, to fit the experimentally measured values of $\tan(\Psi)$ and $\cos(\Delta)$. Herein, we provide a discussion of the factors that govern the optical properties of the monolayer HGNs, emphasizing the morphologies and particle densities on the substrates. We also offer a quantitative comparison of the values of *n* and *k* between solid Au NPs and HGN monolayers. Finally, we demonstrate a simple, highly sensitive chemical sensor prepared through surface modification of metal NPs immobilized on a Si substrate.

RESULTS AND DISCUSSION

We prepared HGNs through the reaction of aqueous $HAuCl_4$ solutions with Ag NPs as templates.[10] Figure 1 reveals that the morphologies of the metal NPs, including spheres, seamless hollow particles, and shells with pinholes, could be controlled by changing the volume of $HAuCl_4$. The as-prepared Ag NPs were solid spheres having an average diameter of *ca.* 27 nm (Figure 1A). When a small amount of $HAuCl_4$ solution was added, the Ag started to dissolve to generate holes on some of the active sites. The dissolution of Ag transformed each Ag NP into an HGN, with holes on its surface and small voids (Figure 1B). After more $HAuCl_4$ solution had been introduced, seamless hollow particles formed with uniform and homogeneous walls (Figure 1C). Moreover, Figure 1D reveals the presence of pinholes on the surface of an HGN. These holes originated from the so-called dealloying process.[26] More porous HGNs formed after increasing the volume of added $HAuCl_4$. Finally, an excessive amount of $HAuCl_4$ led to solid Au spheres forming from the hollow structures (Figure 1E), through collapse of the HGNs. To investigate the optical properties of monolayer HGNs, we allowed the HGNs to self-assemble through chemical adsorption onto Si substrates that we had modified to present NH_2 groups. Figure 1F displays a typical SEM image of an HGN-deposited Si substrate at saturation. The number density was *ca.* 350 particles μm^{-2}; the surface coverage was *ca.* 22%.

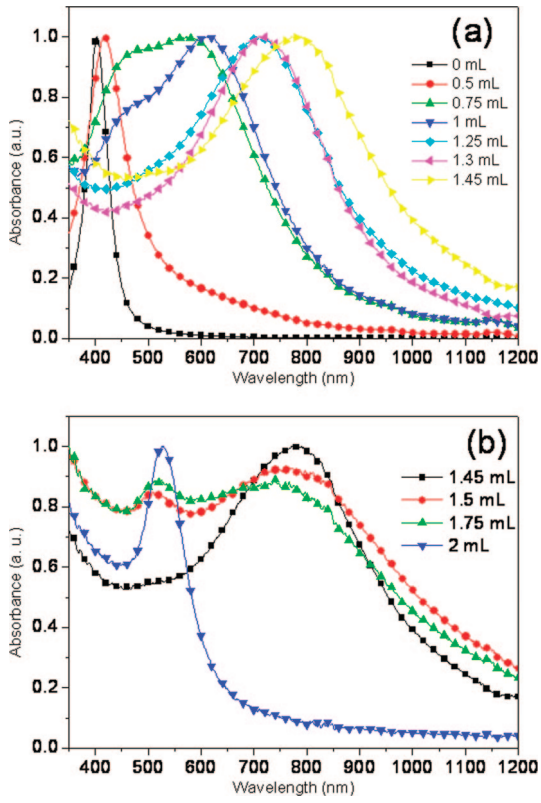

Figure 2. UV−vis−NIR absorbance spectra of aqueous dispersions of Ag NPs before and after reactions with different volumes of 2 mM aqueous $HAuCl_4$. On the basis of the spectral changes, the replacement reaction could be separated into two stages: (a) formation of HGNs; (b) fragmentation of the HGNs into discrete nanostructures. All spectra have been normalized against the intensities of their strongest peaks.

Because Ag, Au NPs, and HGNs often exhibit different SPR peaks in the UV−vis−NIR wavelength region,[4] we could monitor the replacement reaction between the Ag NPs and the $HAuCl_4$ solution using absorption spectroscopy. Figure 2 displays the UV−vis absorbance spectra recorded from aqueous dispersions of Ag NPs after they had reacted with various volumes of the $HAuCl_4$ solution. The Ag NPs exhibited a typical SPR peak at *ca.* 400 nm (black line in Figure 2a). After we added a small amount of the $HAuCl_4$ solution (<0.5 mL), the SPR peak underwent a slight red shift as a result of the Au layer forming on the surfaces of the Ag NPs. This peak decreased in intensity, and signals at longer wavelengths (>600 nm) exhibited significant increases in intensity after we added more $HAuCl_4$ solution to the reaction system. The peak for the Ag NPs disappeared after 1.25 mL of the $HAuCl_4$ solution had been introduced (cyan line in Figure 2a), indicating the formation of HGNs possessing complete shells; meanwhile, the signal at long wavelength underwent a red shift to *ca.* 710 nm. As more $HAuCl_4$ was added, the SPR peak redshifted continuously, owing to the larger void sizes, thinner dimensions of the shells, and the formation of pinholes. The peak underwent a further red shift to *ca.* 790 nm when 1.45 mL of the $HAuCl_4$ solution was added to the reaction mixture (yellow line in Figure 2a). The suspension displayed a color change from dark blue to purplish red when the Ag NPs were reacted with 2 mL of the $HAuCl_4$ solution. The blue line in Figure 2b reveals that the signal blue-shifted back to *ca.* 520 nm, and the peak at NIR wavelength disappeared. These spectral changes indicated that the HGNs had collapsed into solid Au NPs with small fragments. Our TEM images and absorbance spectra are consistent with those reported in the literature.[27] It is noteworthy that the surface plasmons on these metal NPs still behaved as dipoles, even though the various SPR extinction phenomena arose from different morphologies, resonance modes, and compositions.

To determinate the optical constants of monolayer HGNs presenting different morphologies, we fixed the immersion time of the Si substrates for the various samples and estimated that the HGN monolayers had similar particle number densities. We used a spectroscopic ellipsometer to measure the ellipsometric parameters [tan(Ψ) and cos(Δ)] of these samples within the range of wavelengths from 300 to 880 nm and at an incident angle of 75°. Next, we used a three-layer model, consisting of the ambient, the NP layer, and the substrate, to fit the measured values of tan(Ψ) and cos(Δ). The values of *n* and *k* of the HGN monolayers were set as fitting variables and evaluated from fitting curves. Figure 3 displays the *n* and *k* curves obtained with fitting of low-mean-square errors. Typically, one or two pronounced extinction peaks appeared in all of the *k* curves in Figure 3b. After we had added 0.5 mL of the $HAuCl_4$ solution, the curve displayed an extinction peak at 432 nm. The curves of the samples prepared after adding 0.75 and 1 mL of the $HAuCl_4$ solution each display two weak extinction peaks: one at *ca.* 450 nm and the other at a longer wavelength (640 and 664 nm, respectively). The two curves of the samples obtained after adding 1.3 and 1.45 mL of the $HAuCl_4$ solution each present only one peak over the entire spectral region. The most red-shifted extinction peak appeared at 864 nm, with the *k* value of 0.227. After we added more $HAuCl_4$ solution (1.75 mL), the peak at long wavelength decreased in intensity and a weak peak appeared at 528 nm. The curve obtained after adding 2 mL of the $HAuCl_4$ solution displays no peak at the long wavelength and only one peak at shorter wavelength (548 nm; dark yellow line in Figure 3b); this signal had the highest value of *k*. All of the values of *k* were low, except for those in the SPR extinction region, indicating that this material selectively absorbed and scattered incident light at specific wavelength bands. The variations in the trend of the *k* curves are in good agreement with those of the absorption spectra of the same HGNs in aqueous solution (Figure 4a). Thus, the pronounced extinction peaks resulted from the dipole plasmon resonance of these HGNs. We suspect that the slight red shift occurred because the Si substrates had

higher refractive indexes than that of water.[28] Our results reveal that we can indeed use SE to observe the optical behavior of HGN monolayers.

Figure 3a displays the refractive index curves of our HGN monolayers. The *n* curves were highly affected by the *k* curves: in the nonabsorbed region ($k = ca.\ 0$), the refractive index remained constant (between 1.0 and 1.6) for the various samples; in the absorbed region ($k > 0.05$), the refractive index curves exhibited abnormal dispersion behavior.[29] It is interesting that the value of *n* at 300 nm was different for each of the samples, even when the wavelength was located in the nonabsorbed region, as indicated in Figure 4b, which also displays the particle density for each sample with respect to the amount of $HAuCl_4$ added. Because these samples were immersed in the HGN solutions for the same duration, they should have similar densities, except for the case in which the HGNs had collapsed into solid Au NPs with small fragments. The formation of a greater number of smaller solid Au NPs led to higher concentrations of the colloidal solutions and higher particle densities on the Si substrates after 1.75 and 2 mL of the $HAuCl_4$ solution were added. Moreover, the curve for the values of *n* at 300 nm is very similar to that of the particle density, both plotted with respect to the amount of $HAuCl_4$ added; indeed, the value of *n* correlated strongly with the particle density (see the inset to Figure 4b).

To further investigate the correlation between the particle density and the optical properties of the metal NPs, we examined the behavior of Ag NPs having an average diameter of *ca.* 42 nm. We adjusted the immersion time of the Si surfaces to control the particle density of the Ag NPs. Figure 5 displays the measured ellipsometric parameters and optical constants of the monolayer Ag NPs. The tan(Ψ) and cos(Δ) curves exhibit obvious increases in the peak intensity upon increasing the immersion time. This result agrees with the previously reported behaviors of Au NPs.[23] When the immersion time was greater than 6 h, these curves displayed similar features, indicating that the Ag NPs were almost saturated on the surfaces. It is difficult, however, to directly suggest a clear physical meaning for the blue shift in the ellipsometric parameter curves. Therefore, we fitted the parameters and found the optical constants mentioned above; panels c and d in Figure 5 present the *n* and *k* curves of the samples. The extinction peak present in the *k* curves also increased in intensity when the samples were immersed for longer times. All of the extinction peaks were located at *ca.* 440 nm without shift, revealing the SPR phenomenon of the Ag NPs. The strong extinction peaks also caused the *n* curves to exhibit an abnormal dispersion in the absorbed region. Moreover, the value of Δn (*i.e.*, $n_{max} - n_{min}$) increased consistently with respect to the intensity of the extinction peak in the *k* curves. It is noteworthy that the values of *n* varied slowly in the nonabsorbed region ($\lambda > 650$ nm) and grew with increasing

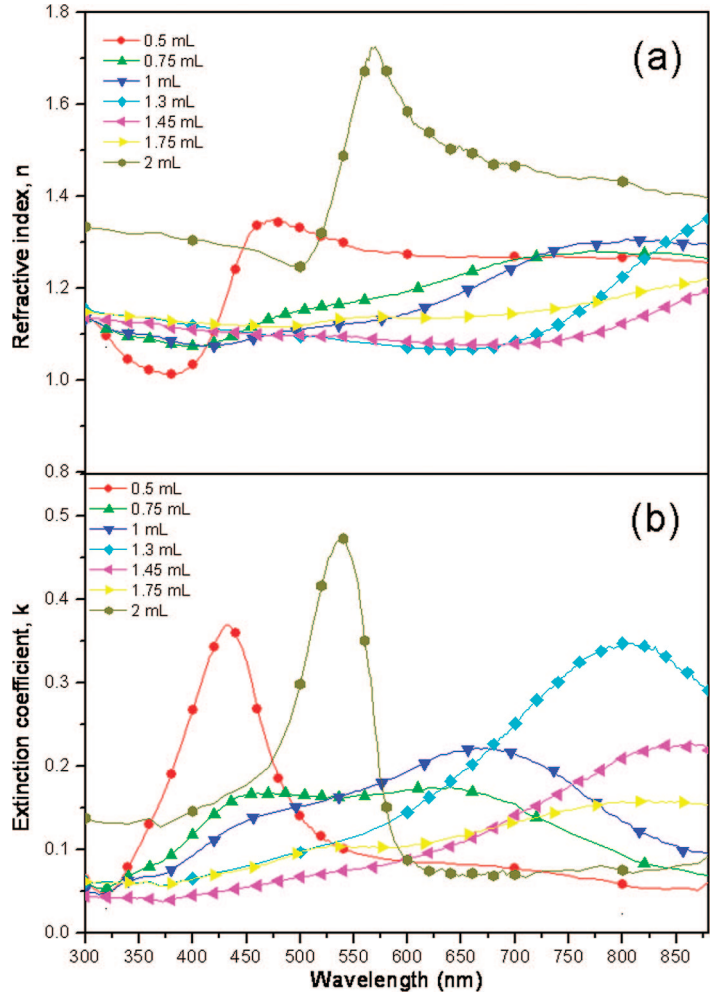

Figure 3. (a) Refractive indices and (b) extinction coefficients, determined from the ellipsometric parameters, of monolayers of the HGNs prepared through reactions with various volumes of the aqueous $HAuCl_4$ solution.

immersion time. The values of *n* ranged from 1.06 to 1.20; they were much higher than that of bulk Ag (*e.g.*, $n = 0.04$, $\lambda = 826$ nm).[30]

We also deposited the HGNs having a diameter of *ca.* 42 nm on the Si substrates through controlling the immersion times from 1 to 52 h. Figure 6 displays the measured ellipsometric parameters and fitted optical constants of the monolayer HGNs. Similar to the situation described above, the tan(Ψ) curves display an obvious peak located at *ca.* 730 nm. The intensity of this signal also increased upon increasing the immersion time (Figure 6a). Unlike the cos(Δ) curves of Ag NPs, however, the cos(Δ) curves of the HGNs presented a broad peak with no enhancement in intensity upon increasing the immersion time (Figure 6b). We suspect that this result arose due to the intrinsic limit of the value of cos(Δ). We might, however, expect to observe such a tendency in the intensity at shorter wavelength (*e.g.*, $\lambda < 400$ nm) upon increasing the immersion time. Figure 6c,d displays the *n* and *k* curves of monolayer HGNs prepared with different immersion times. Because the SE used in this work could only measure the

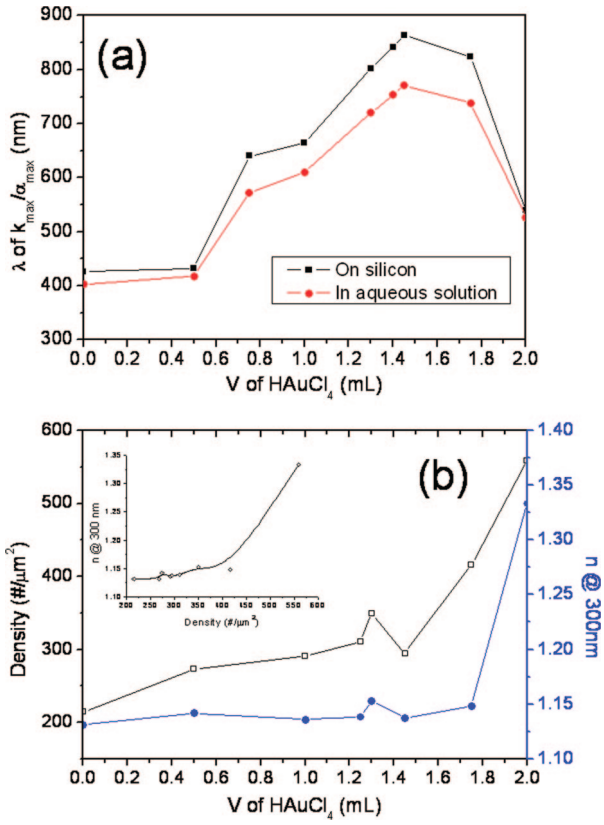

Figure 4. (a) Relationship between the SPR peak wavelength of HGNs on a Si substrate (square) or in aqueous solution (circle) and the volume of the $HAuCl_4$ solution added during the HGN synthesis. (b) Relationships between the volume of the $HAuCl_4$ solution added during the HGN synthesis and, respectively, the particle number density (square) and the value of n at $\lambda = 300$ nm (circle) of HGNs on a Si substrate. Inset: Relationship between the particle number density and the value of n at $\lambda = 300$ nm for HGNs on Si substrates.

samples at wavelength of less than 880 nm, the features of these curves could not be determined completely. Nevertheless, we could still observe the characteristic peaks in the k curves. In addition, the extinction peaks developed and displayed an obvious red shift (from 740 to 870 nm) upon increasing the immersion time (Figure 6d). The red-shift phenomenon might be attributable to the coupling effect due to the neighboring HGNs.[31] It is interesting that the values of n_{min} decreased in the absorbed region (*e.g.*, $\lambda = 700$ nm) owing to the stronger abnormal dispersion induced by the k values. In contrast, the values of n increased in the nonabsorbed region (*e.g.*, $\lambda = 300$ nm) because of the higher particle density.

Figure 7a−f displays SEM images of the HGNs deposited on Si wafers for various immersion times. Figure 7g presents the relationship between the immersion time and the particle number density, as determined from the SEM images. The particle number density exhibited a linear correlation with respect to the immersion time before saturation and after reaching saturation. In addition, the value of k_{max} also displayed a high correlation with respect to the immersion time. Figure 7h reveals the linear correlation between the particle number density and the value of k_{max}. It is noteworthy that the value of n_{min} also correlates significantly with respect to the particle number density. In general, a change in $\cos(\Delta)$ is more obvious than a change in $\tan(\Psi)$ for a thin layer of a deposited material. Therefore, previous studies of the relationship between the ellipsometry parameters and the particle number density for Au NPs have focused on the change in $\cos(\Delta)$.[23−25] Because it is more difficult to observe such a trend in the values of $\cos(\Delta)$ for HGNs, we suggested that the change in $\tan(\Psi)$ near the position of the SPR peak is more suitable for HGNs of various particle number densities (see Figure 6a,b).

Clearly, the HGN monolayers exhibit distinct differences from the optical properties of bulk Au. Generally, metals such as Au or Ag exhibit large values of k because of their conductive characteristics and have very low values of n (typically, $n < 0.4$ at $\lambda = 550-1000$ nm).[30] In contrast, our HGN monolayers possess relative large values of n (typically 1−1.5) but small values of k. Moreover, a pronounced peak was present in the k spectra and an abnormal dispersion appeared in the n spectra associated with the SPR band of these HGNs. In addition, we found that the particle number density had a strong effect on the optical behavior of these HGN monolayers. Because the surface plasmon of the HGNs can be considered as an oscillating dipole, the Lorentz oscillator model[29] (usually used for insulator materials) could be introduced to successfully explain the optical behavior of the HGN monolayers. If the HGNs interact with an external electromagnetic wave at the wavelength associated with their SPR position, then we would expect to observe the resonance absorption phenomenon. Because this behavior induces large amplitude oscillations, the HGNs can, therefore, absorb energy from the incident light. If the light does not coincide with the SPR wavelength, then the HGNs will not the absorb energy. In this situation, the light wave drives nonresonant oscillations of the HGNs and has a smaller propagation velocity than that in free space. The reduction of the velocity is characterized by the refractive index. Therefore, more HGNs result in more oscillating sites in the medium, enlarging the values of k in the absorbed wavelength region and the values of n in the nonabsorbed wavelength region. This tendency agrees with our experimental results mentioned above.

Moreover, we measured the optical constants for HGNs linked on a Si substrate with saturation and compared these values with those for solid Au NPs. Because the particle number density is a major factor in determining the refractive index, we tuned the immersion times to obtain similar densities for the two kinds of samples. Figure 8a displays the curves of the optical constants for HGNs (diameter = 27 nm) and solid Au

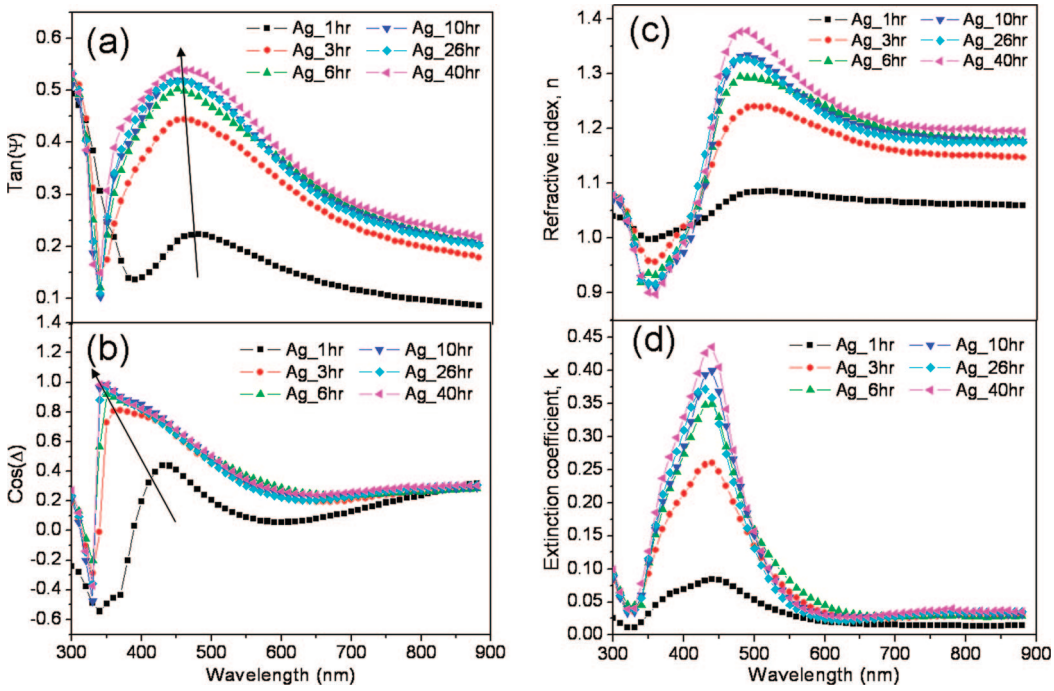

Figure 5. Measured ellipsometric parameters (a) tan(Ψ) and (b) cos(Δ) and calculated values of (c) refractive index and (d) extinction coefficient for Ag NP-adsorbed Si wafers prepared over various immersion times.

NPs (diameter = 20 nm), each with a particle density of *ca.* 350 particles μm^{-2}. First, we compared the values of *n* at wavelengths in the nonabsorbed wavelength region. The solid Au NPs displayed slightly higher values of *n* than those of the HGNs in the nonabsorbed region, even through the particle density was similar, possibly because of the difference in metal volume between the solid Au NPs (Au) and the HGNs (Au and air). Because bulk Au films have values of *n* larger than 1.5 in the wavelength range from 300 to 450 nm,[30] when incident light interacted with the monolayer NPs, the solid Au NPs displayed a higher effective refractive index than did the HGNs. In addition, Figure 8a reveals that the value of k_{max} of the HGNs (0.34 at 802 nm)

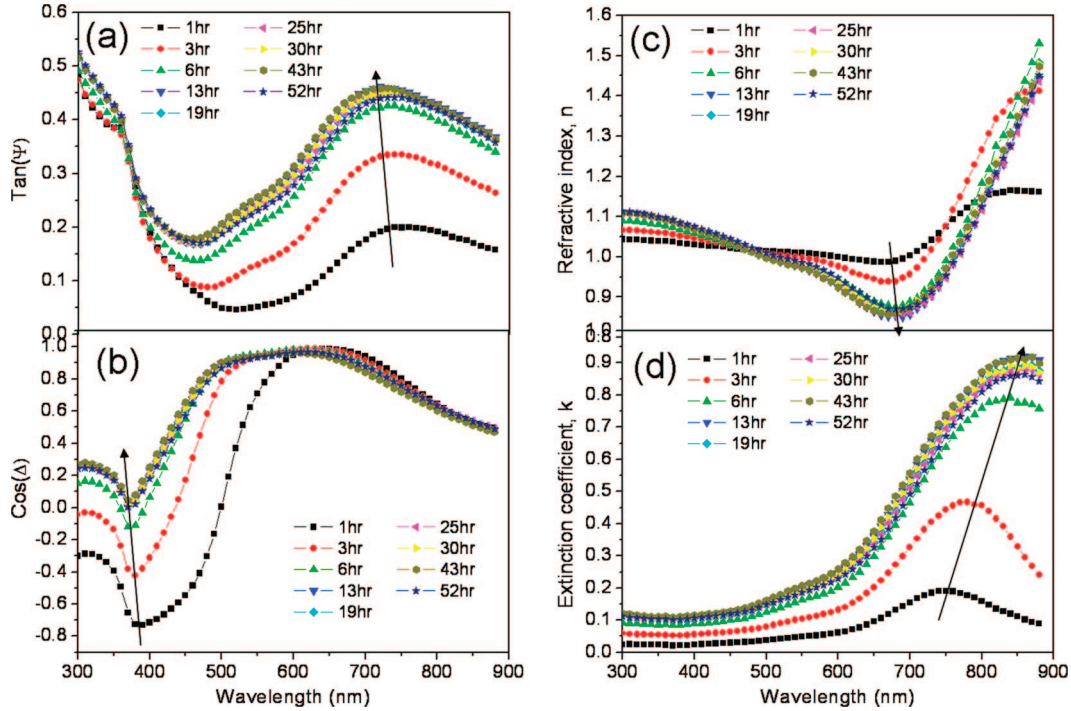

Figure 6. Measured ellipsometric parameters (a) tan(Ψ) and (b) cos(Δ) and calculated values of (c) refractive index and (d) extinction coefficient for HGN-adsorbed Si wafers prepared over various immersion times.

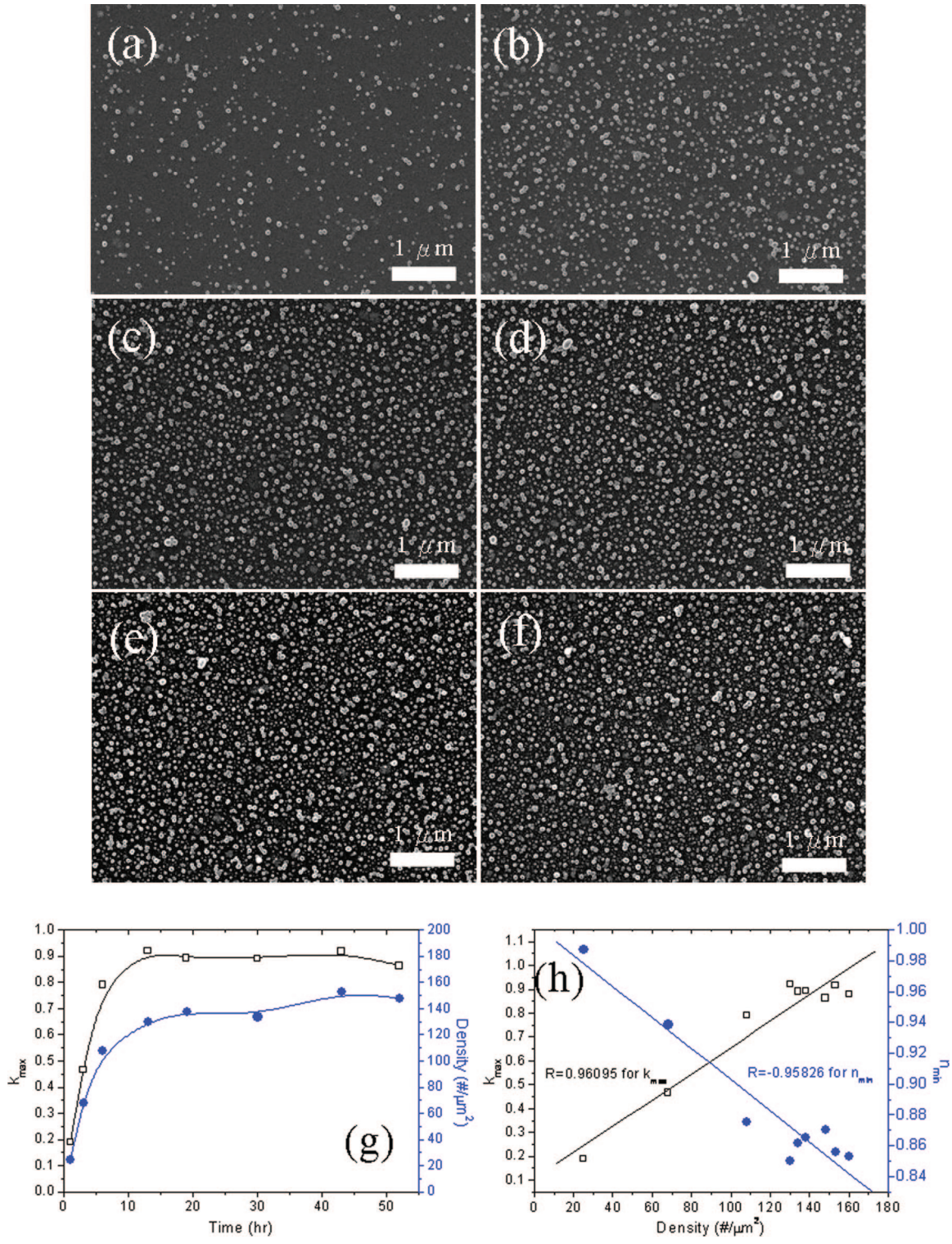

Figure 7. Top-view SEM images of Si wafers loaded with HGNs for (a) 1, (b) 3, (c) 6, (d) 13, (e) 25, and (f) 43 h. (g) Relationship between the immersion time of the HGNs on Si substrate and, respectively, the values of k_{max} (square) and the particle number density (circle). (h) Relationship between the particle number density of the HGNs on Si substrates and, respectively, the values of k_{max} (square) and n_{min} (circle).

was lower than that of the solid Au NPs (0.43 at 545 nm) in the respective SPR wavelength regions. This phenomenon might be attributable to the difference in the intrinsic SPR extinction efficiency between an HGN and a solid Au NP. Calculations performed according to the Mie theory have suggested that a solid Au NP has almost twice the extinction efficiency of an HGN of equal diameter.[32] On the other hand, the SPR extinction efficiency is also sensitive to the size of particles.[9,34] When the particle size is increased, the greater degree of scat-

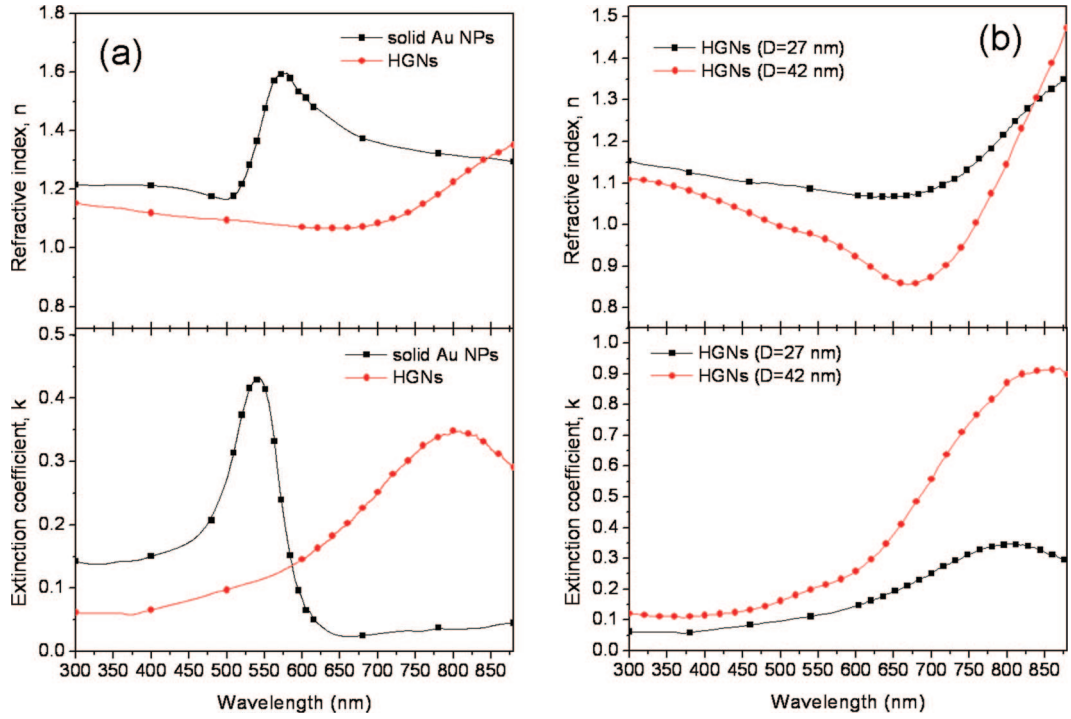

Figure 8. (a) Measured optical constants for solid Au NPs (square) and HGNs (circle) adsorbed on Si substrates at a particle number density of *ca.* 350 particles μm^{-2}. (b) Measured optical constants of HGNs [average diameters = 27 (square) and 42 nm (circle)] adsorbed on Si wafers at saturation.

tering results in a higher extinction efficiency. In our case, the HGNs had slightly larger diameters than did the solid Au NPs; therefore, we would expect the former to possess a value of k slightly higher than half of that of the solid Au NPs. Furthermore, we compared the optical constants at saturation for HGNs possessing average diameters of 27 and 42 nm (Figure 8b). When the samples reached saturation on the Si substrates, the smaller-sized HGNs had a higher particle density (*ca.* 350 particles μm^{-2}) than that of the larger HGNs (*ca.* 150 particles μm^{-2}). This result agrees with that found in the n curves in Figure 8b, where the smaller HGNs displayed a higher value of n at 300 nm ($n = 1.15$) than that ($n = 1.1$) of the larger ones. It is interesting, however, that the larger HGNs provided a dramatically higher value of k_{max} (0.92 at 870 nm) than did the smaller ones (0.34 at 802 nm), even when the former had a much smaller particle density. This behavior indicates that the values of k might be more sensitive to the particle size than to the particle density.

We also compared the values of the optical constants of our monolayer HGNs with those reported previously for solid Au NPs.[20−22,25] For instance, Evans[21] characterized very high refractive index values ($n_{max} = 2.6$; $k_{max} = 1.4$) for self-assembled Au NPs, although we note that their Au NP film was a 12-layer structure rather than a monolayer, so their results are not directly comparable with ours. We can, however, compare our results with those for the optical constants ($n < 1.2$; $k < 0.15$) reported by Kooij *et al.*[20] for monolayer Au NPs. Previously, we reported[22] much higher values for the optical constants of monolayer Au NPs than those reported by Kooij. For a saturated monolayer of Au NPs having a diameter of *ca.* 10 nm, we obtained a maximum refractive index and extinction coefficient of *ca.* 1.9 and 1.2, respectively. We suspect that the difference arose due to the lower surface coverage of their monolayer Au NPs. In addition, Lin *et al.*[25] recently reported values of n and k for monolayer Au NPs that are comparable to ours. As indicated in Figure 8b, we could increase the value of k of the HGNs to 0.92 through increases in the size and density of the particles. Although our highest value of k is still slightly lower than that reported previously for solid Au NPs,[22] the values of k for our HGNs in the SPR absorbance region are high enough for them to serve as sensors.

Generally, a UV−vis transmission measurement is used to monitor a typical glass-based SPR sensor.[33] To develop an applicable SPR-based chip, a conductive or nontransmitting substrate might be necessary. Here, however, we demonstrate a simple concept: relating the device sensitivity to changes in the surrounding medium, using solid Au NP and HGN monolayers on a Si substrate. Because of the high absorption of Si over the whole visible wavelength region, we used the reflectance spectrum and SE to observe the sensitivity. It is worthy to be noted that SE usually could present more details and slight changes of optical properties of a thin film than common transmission or reflection measurement. The

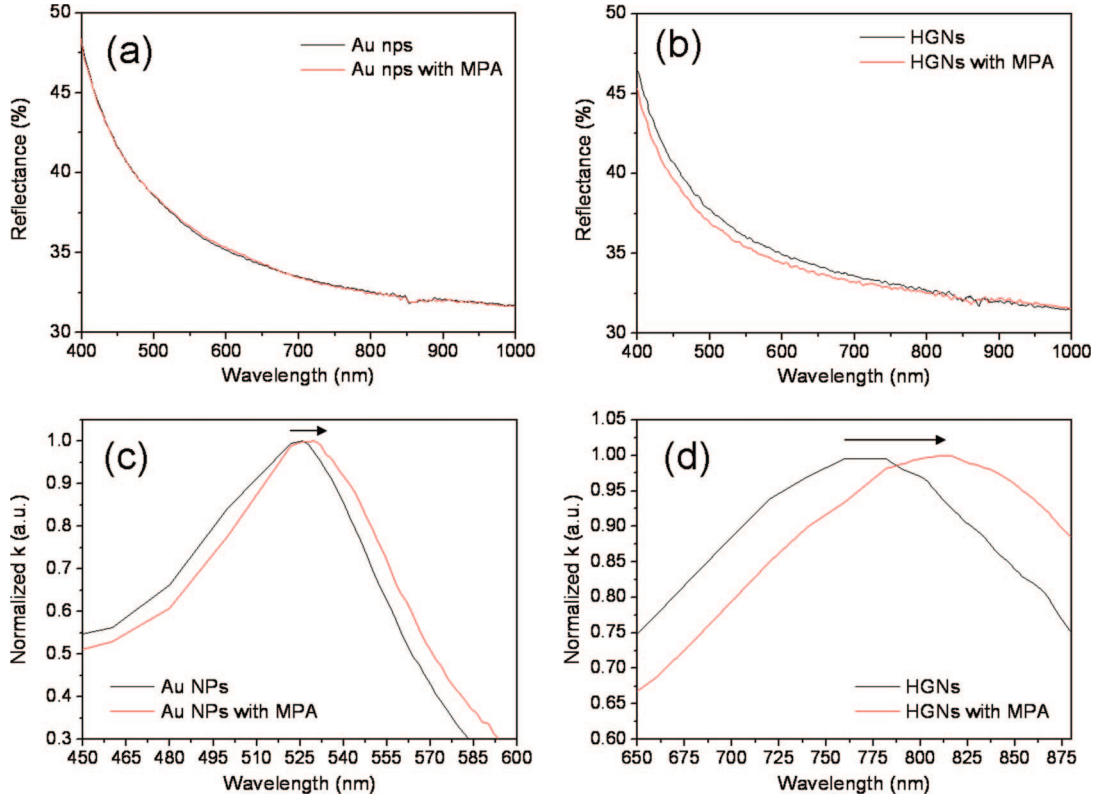

Figure 9. (a,b) Reflectance and (c,d) extinction coefficient spectra of (a,c) Au NP and (b,d) HGN monolayers before (black) and after (red) surface modification with added MPA.

reason could be attributed to the fact that SE collects the change in polarization state of light reflected from the surface of a sample, such as amplitude and phase. Figure 9 displays the reflectance and normalized extinction coefficient spectra of saturated solid Au NP and HGN monolayers before and after binding MPA molecules. Figure 9a,b reveals that no apparent characteristic features appeared in the reflectance spectra, even though extremely slight changes occurred in the curves of the both samples before and after binding MPA molecules. In contrast, the extinction coefficient curves display very distinct SPR peaks (Figure 9c,d). Under the same experimental conditions, the peak for the solid Au NP monolayer displays a red shift from 526 to 530 nm; that for the HGN monolayer displays an obviously larger red shift from 780 to 814 nm. The SPR sensitivity of the HGNs, relative to that of solid Au NPs, was almost 8-fold, possibly because the hollow structure allowed the MPA molecules to diffuse freely into the interior regions of the HGNs and self-assemble to form a monolayer on both the inner and outer faces of the shells.[10] The greater number of bound MPA molecules induced a larger change in the optical constant of the medium surrounding the HGNs. This behavior would cause the SPR peak of the HGNs to undergo a larger red shift. Thus, the HGNs are more suitable for use as SPR sensors than are the solid Au NPs because the former have the same chemical affinity yet higher sensitivity to the surrounding change. In addition, we suggested that SE measurements are useful for measuring the sensitivity of a conductive or nontransmitting SPR sensor.

CONCLUSIONS

We prepared a series of the monolayer HGNs possessing various morphologies and investigated in detail the optical constants (values of n and k), determined using spectroscopic ellipsometry, of their self-assembled monolayers immobilized on Si substrates. The samples exhibited SPR peaks in their k curves that were comparable with those of the same particles in aqueous solution. Furthermore, we use the Lorentz oscillator model to explain the behavior of these HGN monolayers. In the absorbed region, the values of k increased upon increasing the particle number density, reaching a maximum of 0.92; the n curves displayed an abnormal dispersion associated with the strong SPR extinction. In the nonabsorbed region, a relatively larger value of n occurred than that found for bulk Au; it increased upon increasing the particle number density. In addition, we compared the optical constants for monolayers of HGNs and solid Au NPs with similar particle densities. The higher value of k_{max} for the solid Au NP monolayer than that of the HGN monolayer was due to the former's larger extinction efficiency at the SPR wave-

length. Finally, we found that HGN monolayers display a greater sensitivity to changes in their surroundings than do their corresponding solid Au NP monolayers. As a result, HGNs monolayers appear to be particularly useful when incorporated into SPR-based sensors or SPR chips measured using SE.

METHODS

Materials. All chemicals were used as received, without any further purification. Sodium citrate (99%), silver nitrate ($AgNO_3$, 99%), hydrogen tetrachloroaurate ($HAuCl_4$, 99.999%), polyvinylpyrrolidone (PVP, M_w = *ca.* 30K), 3-aminopropyltrimethoxysilane (APTMS), 3-mercaptopropanoic acid (MPA, 99%), methanol (MeOH, 99.5%), ethanol (EtOH, 99.8%), and ethylene glycol (EG, 99.8%) were obtained from ACROS. The Au colloid solution (20 nm) was obtained from Aldrich. Si wafers were obtained from Summit-Tech Co.

Colloid Preparation. HGNs were prepared through the reaction of $HAuCl_4$ with Ag NPs, similar to the method published by Sun and Xia.[10] Briefly, $AgNO_3$ (0.04 g) and PVP (1 g) were dissolved in EG (20 mL). This mixture was heated at 160 °C for 2 h under vigorous magnetic stirring and then cooled to room temperature. The resulting Ag colloid prepared using the polyol method formed stable dispersions in water without the need to add additional stabilizers. The solution of the Ag NPs (1 mL) was diluted in deionized water (25 mL) and then heated under reflux for 10 min before a specific volume of 2 mM aqueous $HAuCl_4$ was added dropwise. A color change—sequentially from yellow to colorless to dark blue—occurred during the course of the replacement reaction. After 20 min of stirring, the particles were cooled to room temperature, purified through gradient centrifugation, washed twice with 0.3 mM aqueous sodium citrate, redispersed in 0.3 mM sodium citrate (5 mL), and finally stored at 4 °C.

HGN Monolayer Preparation. Clean, polished Si substrates were immersed for 45 min in boiling solution of 2% (v/v) of APTMS in anhydrous EtOH. The substrates were then rinsed thoroughly with MeOH to remove any unbound monomer from the surface. At this point, the silanized substrates were stored in MeOH until required. Prior to derivatization with colloidal NPs, the substrates were rinsed with ultrapure water (UPW) and immersed in vials of NPs for lengths of time from 1 to 52 h. The NP-deposited substrates were then spun at 3000 rpm to remove any excess NPs. After performing a final UPW rinse, the samples were dried and stored under ambient conditions until required for further use.

Modification With MPA. The Si substrates were immersed until saturation in a solution of the solid Au NPs or the HGNs. The samples were then immersed in the same solution of MPA in EtOH (50 mM) for 4 h. After performing a final EtOH rinse, the samples were dried and stored under ambient conditions.

Characterization. The absorption and reflectance spectra were recorded using a Hitachi U4100 optical spectrometer. The sizes of NPs were measured using a Philips Tecnai F20 G^2 field emission tunneling electron microscope (FEI-TEM). The NP-deposited substrates were observed using a JEOL JSM-6500F scanning electron microscope (SEM). The ellipsometric parameters of the NP-deposited substrates were measured using a SOPRA SE5E spectroscopic ellipsometer (SE). Measurements were preformed at wavelengths between 300 and 880 nm at a fixed incident angle of 75°. SE measures the change in polarization state of light reflected from the surface of a sample in terms of Ψ and Δ, which are related to the ratio of total reflection coefficients, R^p and R^s for p- and s-polarized light, respectively, according to the expression[37]

$$q = \tan\Psi e^{i\Delta} = \frac{R^p}{R^s}$$

That amplitude of $q = R^p/R^s$ is given by $\tan(\Psi)$, and the difference of the phase between p- and s-polarized components is related to $\cos(\Delta)$. On the other hand, a relation between total reflection coefficients and complex refractive index ($N_2 = n - ik$) of a thin film coated on the substrate is

$$R^p = \frac{r_{12}^p + r_{23}^p \exp(-i2\beta)}{1 + r_{12}^p r_{23}^p \exp(-i2\beta)} \quad R^s = \frac{r_{12}^s + r_{23}^s \exp(-i2\beta)}{1 + r_{12}^s r_{23}^s \exp(-i2\beta)}$$

where

$$\beta = 2\pi\left(\frac{d_2}{\lambda}\right) N_2 \sqrt{1 - (n_a \sin\varphi / N_2)^2}$$

Here, r_{12} and r_{23} are the Fresnel reflection coefficients for the 1−2 (ambient−film) and 2−3 (film−substrate), respectively. Besides, n_a is the real refractive index of the ambient, and φ is the incident angle.

After the ellipsometry data have been collected, it is necessary to use these data to determine the optical constants. For our NP-deposited substrates, a there-layer model is postulated with value of thickness for the NP layer and values of the optical constants for the NP layer and the substrate. The expected values of ellipsometric parameters [$\tan(\Psi)$ and $\cos(\Delta)$] are calculated and compared with the measured quantities. A regression analysis then refines the choices of values for the optical constants until the difference between the calculated values and the measured values is minimized.

Acknowledgment. We thank the National Science Council, Taiwan, ROC, for supporting this study under Contracts NSC-97-2221-E-002-046-MY3 and NSC-97-2623-7-002-008-ET.

REFERENCES AND NOTES

1. Kelly, K. L.; Coronado, E.; Zhao, L. L.; Schatz, G. C. The Optical Properties of Metal Nanoparticles: The Influence of Size, Shape, and Dielectric Environment. *J. Phys. Chem. B* **2003**, *107*, 668–677.
2. Yguerabide, J.; Yguerabide, E. E. Light-Scattering Submicroscopic Particles as Highly Fluorescent Analogs and Their Use as Tracer Labels in Clinical and Biological Applications. *Anal. Biochem.* **1998**, *262*, 137–156.
3. Orendorff, C. J.; Sau, T. K.; Murphy, C. J. Shape-Dependent Plasmon-Resonant Gold Nanoparticles. *Small* **2006**, *2*, 636–639.
4. Jackson, J. B.; Halas, N. J. Silver Nanoshells: Variations in Morphologies and Optical Properties. *J. Phys. Chem. B* **2001**, *105*, 2743–2746.
5. Selvakannan, P. R.; Sastry, M. Hollow Gold and Platinum Nanoparticles by a Transmetallation Reaction in an Organic Solution. *Chem. Commun.* **2005**, 1684–1686.
6. Novak, J. P.; Nickerson, C.; Franzen, S.; Feldheim, D. L. Purification of Molecularly Bridged Metal Nanoparticle Arrays by Centrifugation and Size Exclusion Chromatography. *Anal. Chem.* **2001**, *73*, 5758–5761.
7. Caruso, R. A.; Antonietti, M. Sol-Gel Nanocoating: An Approach to the Preparation of Structured Materials. *Chem. Mater.* **2001**, *13*, 3272–3282.
8. Kubo, S.; Diaz, A.; Tang, Y.; Mayer, T. S.; Khoo, I. C.; Mallouk, T. E. Tunability of the Refractive Index of Gold Nanoparticle Dispersions. *Nano Lett.* **2007**, *7*, 3418–3423.
9. Hao, E.; Li, S.; Bailey, R. C.; Zou, S.; Schatz, G. C.; Hupp, J. T. Optical Properties of Metal Nanoshells. *J. Phys. Chem. B* **2004**, *108*, 1224–1229.
10. Sun, Y. G.; Xia, Y. N. Increased Sensitivity of Surface Plasmon Resonance of Gold Nanoshells Compared to That of Gold Solid Colloids in Response to Environmental Changes. *Anal. Chem.* **2002**, *74*, 5297–5305.
11. Schwartzberg, A. M.; Oshiro, T. Y.; Zhang, J. Z.; Huser, T.; Tally, C. E. Improving Nanoprobes Using Surface-Enhanced Raman Scattering from 30-nm Hollow Gold Particles. *Anal. Chem.* **2006**, *78*, 4732–4736.

12. Shukla, S.; Priscilla, A.; Banerjee, M.; Bhonde, R. R.; Ghatak, J.; Satyam, P. V.; Sastry, M. Porous Gold Nanospheres by Controlled Transmetalation Reaction A Novel Material for Application in Cell Imaging. *Chem. Mater.* **2005**, *17*, 5000–5005.
13. Chen, J.; Saeki, F.; Wiley, B. J.; Cang, H.; Cobb, M. J.; Li, Z. Y.; Au, L.; Zhang, H.; Kimmey, M. B.; Li, X.; Xia, Y. Gold Nanocages: Bioconjugation and Their Potential Use as Optical Imaging Contrast Agents. *Nano Lett.* **2005**, *5*, 473–477.
14. Jung, L. S.; Campbell, C. T.; Chinowsky, T. M.; Mar, M. N.; Yee, S. S. Quantitative Interpretation of the Response of Surface Plasmon Resonance Sensors to Adsorbed Films. *Langmuir* **1998**, *14*, 5636–5648.
15. Brockman, J. M.; Nelson, B. P.; Corn, R. M. Surface Plasmon Resonance Imaging Measurements of Ultrathin Organic Films. *Annu. Rev. Phys. Chem.* **2000**, *51*, 41–63.
16. Quinn, J. G.; O'Neill, S.; Doyle, A.; McAtamney, C.; Diamond, D.; MacCraith, B. D.; O'Kennedy, R. Development and Application of Surface Plasmon Resonance-Based Biosensors for the Detection of Cell−Ligand Interactions. *Anal. Biochem.* **2000**, *281*, 135–143.
17. Hutter, E.; Fendler, J. H.; Roy, D. Surface Plasmon Resonance Studies of Gold and Silver Nanoparticles Linked to Gold and Silver Substrates by 2-Aminoethanethiol and 1,6-Hexanedithiol. *J. Phys. Chem. B* **2001**, *105*, 11159–11168.
18. Fu, E.; Ramsey, S. A.; Yager, P. Dependence of the Signal Amplification Potential of Colloidal Gold Nanoparticles on Resonance Wavelength in Surface Plasmon Resonance-Based Detection. *Anal. Chim. Acta* **2007**, *599*, 118–123.
19. Li, X.; Tamada, K.; Baba, A.; Knoll, W.; Hara, M. Estimation of Dielectric Function of Biotin-Capped Gold Nanoparticles via Signal Enhancement on Surface Plasmon Resonance. *J. Phys. Chem. B* **2006**, *110*, 15755–15762.
20. Kooij, E. S.; Wormeester, H.; Brouwer, E. A. M.; Vroonhoven, E.; Silfhout, A.; Poelsema, B. Optical Characterization of Thin Colloidal Gold Films by Spectroscopic Ellipsometry. *Langmuir* **2002**, *18*, 4401–4413.
21. Zhang, H.-L.; Evans, S. D.; Henderson, J. R. Spectroscopic Ellipsometric Evaluation of Gold Nanoparticle Thin Films Fabricated Using Layer-by-Layer Self-Assembly. *Adv. Mater.* **2003**, *15*, 531–534.
22. Chen, H. L.; Cheng, H. C.; Ko, T. S.; Chuang, S. Y.; Chu, T. C. Characterizing Optical Properties of Self-Assembled Gold Nanoparticles for Surface Plasmon Resonance Device. Applications. *Jpn. J. Appl. Phys.* **2006**, *45*, 6984–6986.
23. Bhat, R. R.; Genzer, J. Using Spectroscopic Ellipsometry for Quick Prediction of Number Density of Nanoparticles Bound to Non-transparent Solid Surfaces. *Surf. Sci.* **2005**, *596*, 187–196.
24. Chen, M.; Horn, R. G. Refractive Index of Sparse Layers of Adsorbed Gold Nanoparticles. *J. Colloid Interface Sci.* **2007**, *315*, 814–817.
25. Wang, D. S.; Lin, C. W. Density-Dependent Optical Response of Gold Nanoparticle Monolayers on Silicon Substrates. *Opt. Lett.* **2007**, *32*, 2128–2130.
26. Erlebacher, J.; Aziz, M. J.; Karma, A.; Dimitrov, N.; Sieradzki, K. Evolution of Nanoporosity in Dealloying. *Nature* **2001**, *410*, 450–453.
27. Sun, Y.; Xia, Y. Mechanistic Study on the Replacement Reaction between Silver Nanostructures and Chloroauric Acid in Aqueous Medium. *J. Am. Chem. Soc.* **2004**, *126*, 3892–3901.
28. Novo, C.; Funston, A. M.; Santos, I. P.; Liz-Marza'n, L. M.; Mulvaney, P. Influence of the Medium Refractive Index on the Optical Properties of Single Gold Triangular Prisms on a Substrate. *J. Phys. Chem. C* **2008**, *112*, 3–7.
29. Fox, M. *Optical Properties of Solids*; Oxford University Press: New York, 2001; pp 29−34.
30. Palik, E. D.; Ghosh, G. *Handbook of Optical Constants of Solids*; Academic: Orlando, FL, 1985; Vol. 1; pp 286−294; pp 350−356.
31. Khlebtsov, B. N.; Khanadeyev, V. A.; Ye, J.; Mackowski, D. W.; Borghs, G.; Khlebtsov, N. G. Coupled Plasmon Resonances in Monolayers of Metal Nanoparticles and Nanoshells. *Phys. Rev. B* **2008**, *77*, 035440.
32. Schelm, S.; Smith, G. Internal Electric Field Densities of Metal Nanoshells. *J. Phys. Chem. B* **2005**, *109*, 1689–1694.
33. Tam, F.; Moran, C.; Halas, N. Geometrical Parameters Controlling Sensitivity of Nanoshell Plasmon Resonances to Changes in Dielectric Environment. *J. Phys. Chem. B* **2004**, *108*, 17290–17294.
34. Peña, O.; Pal, U.; Rodríguez-Fernández, L.; Crespo-Sosa, A. Linear Optical Response of Metallic Nanoshells in Different Dielectric Media. *J. Opt. Soc. Am. B* **2008**, *25*, 1371–1379.
35. Wu, P. C.; Kim, T. H.; Brown, A. S.; Losurdo, M.; Bruno, G.; Everitt, H. O. Real-Time Plasmon Resonance Tuning of Liquid Ga Nanoparticles by *In Situ* Spectroscopic Ellipsometry. *Appl. Phys. Lett.* **2007**, *90*, 103119.
36. Lee, S. J.; Yu, A. C. C.; Lo, C. C. H.; Fan, M. Optical Properties of Monodispersive FePt Nanoparticle Films. *M. Phys. Status Solidi A* **2004**, *201*, 3031–3036.
37. Tompkins, H. G.; McGahan, W. A. *Spectroscopic Ellipsometry and Reflectometry: A User's Guide*; Wiley: New York, 1999; pp 12−17.